01 Feb 1991

The Synthesis of Patterns using a Series-Fed Array of Annular Sector Radiating Line (ANSERLIN) Elements: Low-Profile, Circularly Polarized Radiators

James L. Drewniak
Missouri University of Science and Technology, drewniak@mst.edu

P. E. Mayes

Recommended Citation

J. L. Drewniak and P. E. Mayes, "The Synthesis of Patterns using a Series-Fed Array of Annular Sector Radiating Line (ANSERLIN) Elements: Low-Profile, Circularly Polarized Radiators," *IEEE Transactions on Antennas and Propagation*, vol. 39, no. 2, pp. 184-189, Institute of Electrical and Electronics Engineers (IEEE), Feb 1991.
The definitive version is available at https://doi.org/10.1109/8.68180

The Synthesis of Patterns Using a Series-Fed Array of Annular Sector Radiating Line (ANSERLIN) Elements: Low-Profile, Circularly Polarized Radiators

James L. Drewniak, *Member, IEEE,* and Paul E. Mayes, *Fellow, IEEE*

Abstract—**A series-fed, circularly polarized (CP) array of annular sector, radiating-line elements is presented. The array operates over a ground plane and has a low profile. Pattern shaping can be achieved through control of the fraction of the incident power that is radiated by each element. This can be accomplished over a wide range by a simple adjustment in the geometry of each element. A synthesis technique is given, and experimental results are presented. The array is demonstrated to have a high return loss (good impedance match) and a low axial ratio.**

I. Introduction

MICROSTRIP patch elements are widely used in antenna arrays that require a low-profile structure over a ground plane. For narrow-band applications a series feed may be satisfactory. Designs of series-fed, linearly polarized, microstrip patch arrays have previously been reported [1]–[4]. The amplitude taper of these arrays is obtained from the patch geometry, and the correct phasing is obtained with the proper length of microstrip line connecting adjacent elements. The simplicity of the series-fed, linearly polarized, microstrip patch array makes it an attractive candidate for applications which require a low-profile, high directivity antenna.

Circular polarization (CP) can be achieved from a microstrip patch antenna with a single feed point, but the CP bandwidth is quite small (less than 4%) [5]. Circularly polarized arrays of microstrip patches with multipoint feeds are quite complicated by contrast to linearly polarized, microstrip patch arrays. One design using linearly polarized elements to produce CP has reduced the number of phase shifters and feed lines [6].

The annular sector, radiating line (ANSERLIN) antenna is a simple, low-profile, traveling-wave, broad-band, CP radiator [7]. This antenna has the property that, within rather broad limits, a specified percentage of the input power can be radiated by choosing the geometric parameters appropriately. Furthermore, the impedance bandwidth of ANSERLIN elements is so large that it should never be the determining factor in the operating bandwidth of any array made from these elements. These properties make the antenna a good candidate for the elements in a series-fed array. In this paper, a design technique and experimental results for a series-fed, CP, linear array are presented. Design curves relate the fractional power that is radiated by the element to the element geometry. The array elements have a high return loss so the return loss for the array is also high.

Manuscript received June 27, 1989; revised February 20, 1990. This work was supported by TRW.

The authors are with the Electromagnetics Laboratory, Department of Electrical and Computer Engineering, University of Illinois, Urbana, IL 61801.

IEEE Log Number 9040704.

II. The ANSERLIN Element

The geometry and operation of the ANSERLIN element is described in detail elsewhere [7], so only a brief description of the properties of the element that are important for array design is given here. A top view of the ANSERLIN array is shown in Fig. 1. For a single element, a 50 Ω annular sector of strip conductor over a ground plane is fed by a triangular fin transmission line of like impedance. The fin transmission line is excited at its small end by a 50 Ω, 0.085-in coaxial cable probe. For single-element operation the output is identical to the input, and is terminated in a nonreflecting load. In this manner the entire antenna is constructed to be a matched, 50 Ω transmission line. The input impedance that results is nearly 50 Ω over a very wide frequency band. A return loss greater than 20 dB has been measured over an 8 : 1 frequency band. For most geometric parameters, the return loss in the radiation pattern bandwidth is greater than 25 dB. It is not essential that the impedance of the antenna be equal to 50 Ω. However, to achieve a pure traveling wave, it is necessary that the entire length of transmission line, i.e., annular sector, fin, and feed probe be of the same impedance, and terminated in a nonreflecting load. Mismatches at any point along the line generate a standing wave component, thereby degrading the input impedance and CP performance of the antenna.

One property of the ANSERLIN antenna that makes it useful as an element in a series-fed array is the increasing radiation loss for increasing Λ, where Λ is the ratio of the outer radius b, to the inner radius a, of the annular sector as shown in Fig. 1. The measured $|S_{21}|$ (in decibels) of the isolated element is plotted in Fig. 2 as a function of Λ, for a constant outer radius of the element of $b = 3.5$ cm. Six values of Λ are shown at nine different frequencies. The relative power that is radiated by the element is $1 - |S_{21}|^2$ (since $|S_{11}| \approx 0$). The approximate linearity of the curves makes the series-fed array design particularly simple. Once the excitation coefficient of a particular element has been related to $|S_{21}|$ as given in the next section, the value of Λ is obtained from Fig. 2. The impedance level, in this case 50 Ω, determines the ratio of the width w of the annular sector of strip conductor, to the height h above the ground plane, for an element with a high return loss. Then, Λ and w/h (and the design frequency) completely determine the geometric parameters of the antenna [7]. The symmetry of the

0018-926X/91/0200-0184$01.00

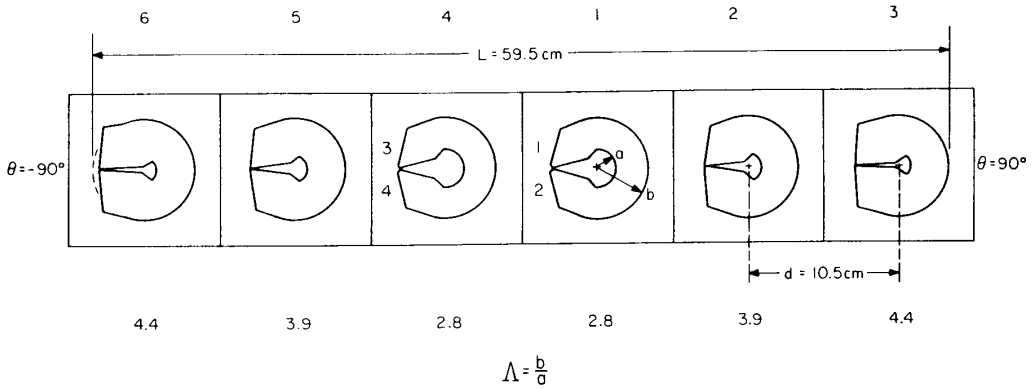

Fig. 1. Array geometry. The input ports of Elements 1 and 4 are numbered for four port measurements.

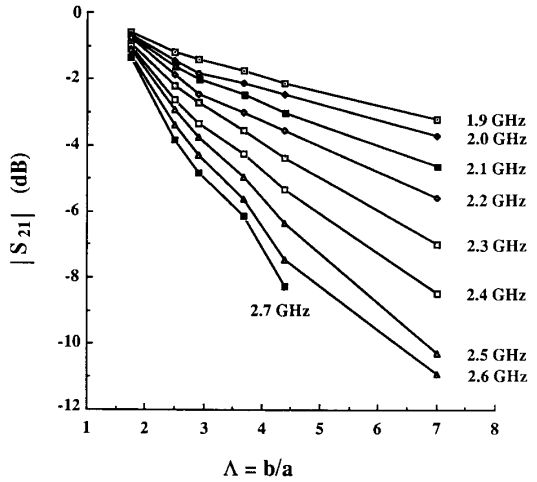

Fig. 2. $|S_{21}|$ versus element geometry ($\Lambda = b/a$), for 50 Ω elements, from two-port measurements of the isolated elements.

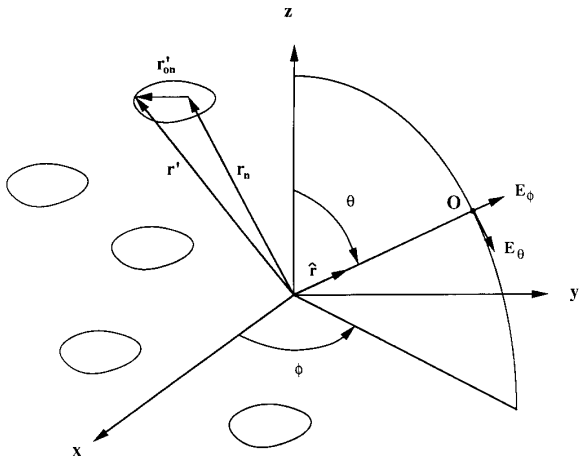

Fig. 3. Coordinate system for the element and array radiation patterns.

element radiation pattern in the symmetry plane of the element, and the wide range of curves in Fig. 2 indicate that broadside linear arrays with a variety of amplitude tapers can be designed using ANSERLIN antennas as elements.

The wave traveling around the annular sector has a phase given by $e^{-jm'\phi}$, where m' depends upon the radius of the annular sector and the frequency. Traveling-wave sources with a phase shift of one degree per degree angle of traversal in azimuth are known to produce a low axial ratio (AR) over an appreciable portion of the single-lobed radiation pattern [8]. Exactly this phase shift ($m' = 1$) is achieved by the ANSERLIN antenna at one frequency [7]. A wide pattern bandwidth is then obtained as m' varies about unity. A figure-of-merit proportional to the power gain is found to be slowly varying over a 30% bandwidth [7]. This will be referred to as the element radiation pattern bandwidth. At the $m' = 1$ frequency, the broadside AR is less than 0.5 dB for element geometries with $2.5 < \Lambda < 4.5$. A broadside AR at the $m' = 1$ frequency of 2.0 dB and 1.0 dB was measured for the elements constructed with $\Lambda = 1.75$ and $\Lambda = 7.0$, respectively. The broadside AR for elements with $2.5 < \Lambda < 4.5$ is on the average 0.5 dB over the radiation pattern bandwidth. Some degradation occurs in the broadside axial ratio at the lower end of the band. A squint of the beam in the plane orthogonal to the plane of symmetry is observed for $m' \neq 1$. However, the beam squint remains less than 10° from broadside over the 30% pattern bandwidth. No beam squint is observed in the symmetry plane of the antenna over the radiation pattern bandwidth.

Although elements of the same outer radius, but different Λ, achieve an $m' = 1$ phase shift at slightly different frequencies [7], the radiation patterns for the different elements are approximately the same over the radiation pattern bandwidth [9]. The radiation patterns in the plane of symmetry of the antenna for the two orthogonal electric field components E_θ and E_ϕ (see Fig. 3) are compared for $\Lambda = 2.5$ and $\Lambda = 4.38$ in Fig. 4. The frequency is 2.2 GHz, which is the design frequency of the array presented in Section IV. The antenna is oriented with the coordinate system of Fig. 3 such that it lies in the xy plane, $\theta = 0°$ is broadside to the antenna, the yz plane is the plane of symmetry, and the ports of the antenna are in the direction of the $-y$ axis. The element radiation patterns shown in Fig. 4 are oriented to the coordinate system of Fig. 3 (a negative sign on θ implies $\pi < \phi < 2\pi$). Due to the limited dynamic range of the measurement system, values less than -25 dB with respect to the beam maximum are assigned a value of -25 dB in Fig. 4 (and similarly in Figs. 6(a) and 6(b)). The relative shapes of the radiation patterns of elements with different Λ compare similarly in other planes.

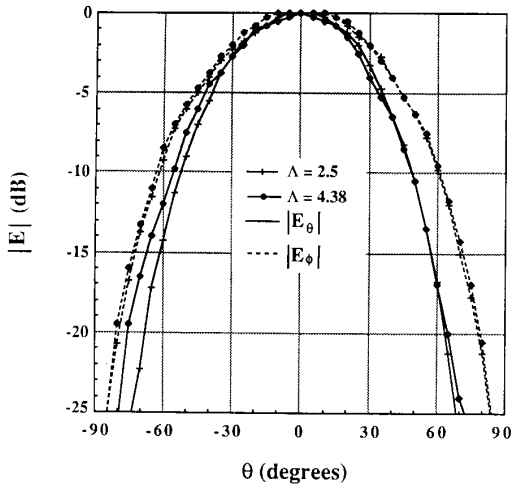

Fig. 4. Comparison of the radiation pattern shapes for $\Lambda = 2.5$ and $\Lambda = 4.38$ at 2.2 GHz. The ordinate has been normalized such that the beam maximum is 0 dB.

III. Excitation Coefficients by Element Geometry

The far-field expression for the electric field of N discrete sources with identical distributions of electric current is given by

$$E = -jk\eta \frac{e^{-jkr}}{4\pi r}\left[\int_{V_1} \mathbf{J}_1(\mathbf{r}'_{01}) e^{jk\hat{\mathbf{r}}\cdot\mathbf{r}_{01}}\, dv'\right] \sum_{n=1}^{N} I_n e^{jk\hat{\mathbf{r}}\cdot\mathbf{r}_n} \quad (1)$$

where $\mathbf{r}_n$ is the position vector to a reference point on the nth element as shown in Fig. 3, $\mathbf{r}'_{on}$ is the position vector from the reference point on the nth element to a source point on that element, $\hat{\mathbf{r}}$ is the unit radial vector of spherical coordinates, r is the distance from the origin of the coordinates to the observation point O, $k = \omega\sqrt{\mu_0\epsilon_0} = 2\pi/\lambda$ is the free-space phase constant, η is the free-space wave impedance, $\mathbf{J}$ is the current density on the elements in the array when the input current is $1\angle 0°$, I_n is the complex amplitude of the current at the input terminals of the nth element, and dv' is an element of volume expressed in primed (source) coordinates. The integral is the element radiation pattern and the sum is the array factor.

The factorization given in (1) is the well-known multiplication principle for array design. The array excitation coefficients are given by the I_n. For arrays of one-port elements, knowledge of the self- and mutual impedances enables one to realize the input currents that are prescribed by a synthesis technique in order to achieve a desired pattern. If there is negligible coupling between one-port elements, the contribution of each element to the power in the distant field is proportional to the squared magnitude of the input current [10]. However, in a series-fed array, the elements must be treated as two-ports, and the power that is radiated by each element is only a fraction of the power across the input port. In preparation for utilizing them as elements in series-fed arrays, and for convenience in testing, the ANSERLIN antennas have been characterized by two-port S-parameters. A synthesis technique has, therefore, been developed to realize the excitation coefficients of (1) in terms of S-parameters of cascaded two-port radiators. This is accomplished by relating the magnitude of the mth excitation coefficient to the power that is radiated by the mth element. The above assumption of identical element patterns is not exactly true in the case of the ANSERLIN antenna. However, as illustrated in Fig. 4, even for elements with widely different values of Λ, the difference in the radiation patterns is slight for angles less than 40° off broadside.

Consider the circuit representation of an array of identical one-port elements. The voltage at the input terminals of the mth element is related to the currents at the terminals of all elements by

$$V_m = \sum_{n=1}^{N} Z_{mn} I_n = Z_{mm} I_m + \sum_{n=1}^{N}{}' Z_{mn} I_n \quad (2)$$

where the prime on the summation in (2) indicates that the mth term is not included. The complex power at the terminals of the mth element is given by

$$P_m = V_m I_m^* = Z_{mm} |I_m|^2 + \sum_{n=1}^{N}{}' Z_{mn} I_n I_m^* \quad (3)$$

where Z_{mm} is the impedance observed at the terminals of the mth element in the presence of all other elements terminated in open circuits, and voltages and currents are represented by their effective values. The real part of the summation is the mutually radiated power [10]. When coupling between elements is negligible

$$P_m = Z_{mo} |I_m|^2 \quad (4)$$

where Z_{mo} is the impedance of the mth element when isolated. The average value of the input power at the terminals of the mth element is then

$$\mathrm{Re}[P_m] = |I_m|^2 \mathrm{Re}[Z_{mo}] = |I_m|^2 R_{mo}. \quad (5)$$

If the dissipative losses in the element are neglected, the power radiated by the mth element is equal to the input power. Then, the magnitude of the terminal current at the mth element is related to the power that is radiated by that element as

$$|I_m| = \sqrt{G_{mo}\,\mathrm{Re}[P_m]} \quad (6)$$

where $G_{mo} = [R_{mo}]^{-1}$. If the voltage at the input terminals of an element is used as the excitation coefficient, as might be done for slot elements, a similar relationship can be constructed between the voltage excitation coefficient of the mth element and the square root of the power that is radiated by the mth element. The mth excitation coefficient can also be related to the power that is radiated by the mth element by relating the total power in the radiation field $(\mathbf{E}\cdot\mathbf{E}^*)/\eta$ to the excitation coefficients. If the mutually radiated power can be neglected, and the radiation patterns of the array elements are assumed identical, then the excitation coefficient of the mth element can be shown to be proportional to the square root of the power that is radiated by that element. These conditions are approximately satisfied by a series-fed array of ANSERLIN elements.

Neglecting mutual coupling, the input resistance of each ANSERLIN element can be made the same. It is therefore assumed that an incident wave encounters no discontinuities as it travels from the input port through the array. This requires that the output port of the last element be terminated in a matched load. Then, denoting the mth excitation coefficient as a_m, and relating $|a_m|^2$ to the power that is radiated by the mth element in terms of S-parameters

$$|a_m|^2 = K\left(1 - |S_{21}^m|^2\right) \prod_{p=1}^{m-1} |S_{21}^p|^2, \qquad m \neq 1 \quad (7a)$$

$$|a_1|^2 = K\left(1 - |S_{21}^1|^2\right). \quad (7b)$$

The proportionality factor K is given by

$$\sum_{m=1}^{N} |a_m|^2 = K\left(1 - \prod_{p=1}^{N} |S_{21}^p|^2\right) = Ke_A \tag{8a}$$

$$K = \frac{1}{e_A} \sum_{m=1}^{N} |a_m|^2 \tag{8b}$$

where e_A is the desired ratio of the total power that is radiated to the input power, and is less than unity.

For a symmetric pattern, the array is divided into two sections and the incident power is split to provide equal excitations for each of the two halves. Only half of the array need be considered in the synthesis, the other half resulting as a consequence of the symmetry. Solving (7) for the S-parameters of the elements on one side of a symmetric array, the $|S_{21}^p|$, $p \neq N$, is given by

$$|S_{21}^p|^2 = \frac{K - \sum_{m=1}^{p} |a_m|^2}{K - \sum_{m=1}^{p-1} |a_m|^2} \tag{9a}$$

$$|S_{21}^1|^2 = \frac{K - |a_1|^2}{K}. \tag{9b}$$

When $p = N$

$$|S_{21}^N|^2 = \frac{K(1 - e_A)}{K - \sum_{m=1}^{N-1} |a_m|^2}. \tag{9c}$$

The phase of each excitation coefficient is realized simply by using the appropriate length of transmission line connecting two adjacent elements in the series-fed array.

IV. Array Design

A six-element, series-fed array was designed for a Chebyshev taper with -20 dB sidelobes. The design frequency was 2.2 GHz. A 0.77 λ element spacing was chosen to minimize mutual coupling. The array geometry is shown in Fig. 1. The $|S_{21}^m|$ of the elements were determined using a procedure that is approximately equivalent to the one previously described. If one assumes that the first factor in (7) is a weak function of m (as might be expected for slightly tapered aperture distributions), that factor can be absorbed in the constant K ($K' = K(1 - |S_{21}^m|^2)$) so that (7) becomes

$$|a_m|^2 = K' \prod_{p=1}^{m-1} |S_{21}^p|^2, \qquad m \neq 1$$

$$|a_1|^2 = K'. \tag{10}$$

A simple normalization is to take $|I_1| = 1$ and the Chebyshev synthesis yields $|I_2| = 0.78$, and $|I_3| = 0.54$. Equation (10) then gives $|S_{21}^1| = 0.78 = -2.2$ dB and $|S_{21}^2| = 0.69 = -3.2$ dB, and $|S_{21}^3|$ is set by the power delivered to the matched termination. The power that is radiated by the array is given by

$$e_A = 1 - \prod_{p=1}^{N} |S_{21}^p|^2 \tag{11}$$

and taking $e_A = 0.87$ gives $|S_{21}^3| = 0.67 = -3.5$ dB.

The element geometries were obtained from Fig. 2 and previ-

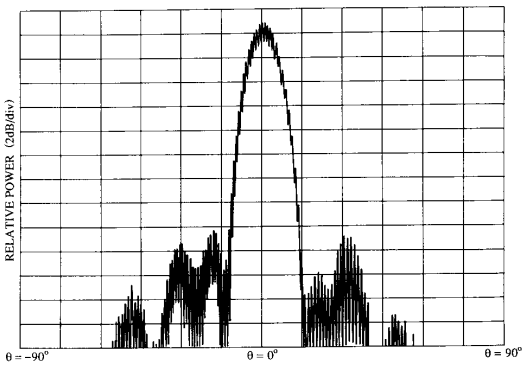

Fig. 5. Radiation pattern in the line of the array at the design frequency of 2.2 GHz measured with a spinning source.

TABLE I
Return Loss and Transmission Parameter of the Isolated Array Elements

	Element Number	$\lvert S_{11}\rvert$ (dB)	$\lvert S_{21}\rvert$ (dB)	$\angle S_{21}$ (degrees)
Right Half	1	−35.5	−2.12	−67.2
	2	−36.4	−2.94	−57.7
	3	−34.8	−3.29	−58.9
Left Half	4	−23.7	−2.14	−72.6
	5	−29.4	−2.96	−55.6
	6	−28.6	−3.39	−61.5

reported design tables [7]. The individual elements were constructed with the annular sector placed above a 10.5 × 10.5 cm, 0.064-in thick ground plane. The two-port parameters of the individual elements mounted on a 14-in × 14-in ground plane were measured. The $|S_{11}|$, $|S_{21}|$, and $\angle S_{21}$ of the elements, referenced to the antenna input terminals, are listed in Table I. There is good agreement between the measured $|S_{21}^m|$ and those prescribed by the design. The percentage of the input power that is radiated by the array is calculated from the $|S_{21}^m|$ ($(1 - |S_{21}^1|^2 |S_{21}^2|^2 |S_{21}^3|^2) \times 100\%$) listed in Table I to be 86%. Negligible mutual coupling has been assumed in calculating this figure.

The array was assembled with the elements placed on a 36-in circular aluminum ground plane. Elements 1 and 4 (Fig. 1) were fed from a matched two-way power divider. The assembly of the right half of the array had port 2 of element 1 connected to port 1 of element 2 by a length of 0.085-in semirigid coaxial cable to yield 0° relative phasing. Similarly, element 2 was connected in series to element 3, and port 2 of element 3 terminated in 50 Ω. The left side of the array was assembled identical to the right. The error in the relative phasing between the elements was measured and found to be less than 7°.

V. Array Performance

The return loss of the matched power divider, with both output ports terminated in 50 Ω, was 36.6 dB at the design frequency of 2.2 GHz. The return loss of the array at the design frequency, 2.2 GHz, seen at the input of the matched power divider, was 26.2 dB, and the voltage standing-wave ratio (VSWR) from 2–3 GHz remained less than 1.22.

An elevation plane radiation pattern in the line of the array, measured with a spinning source, is shown in Fig. 5. The

orientation of the radiation pattern with respect to the array is indicated by $\theta = -90°$ and $\theta = +90°$ in Fig. 1, which corresponds to angles of $-\theta$ and $+\theta$ in Fig. 5. The axial ratio at broadside is 1.6 dB, and remains less than 2 dB on the main beam down to the -10 dB points. The measured 3 dB beamwidth of approximately 12° compares well with the theoretical value of 12.4°. The discrepancy between the measured and designed sidelobe level, lies, in part, in the assumption that the $|S_{21}|$ of all elements is approximately the same, and hence using (10) to determine the excitation coefficients. Other contributions to the difference between the measured and designed sidelobe levels, are the neglect of mutual coupling, and the finite return loss of the elements.

It is apparent from the Λ of the elements given in Fig. 1, and the $|S_{21}^m|$ given in Table I, that the elements are not identical. As a result, some deviation from the theoretical sidelobe level is expected. If (8) and (9) are used with the measured values of $|S_{21}^m|$ of the array elements and $e_A = 0.86$, then $K = 2.209$, and the resulting excitation coefficients are 0.60 : 0.82 : 0.93 : 0.93 : 0.82 : 0.60, as compared with 0.54 : 0.78 : 1.0 : 1.0 : 0.78 : 0.54 calculated from (10). The difference in the normalizations should be recalled. It is seen by computing the array factor for both sets of excitation coefficients that the 3-dB beamwidths differ by only a fraction of a degree; however, as expected, there is a significant difference in the sidelobe level. Measured radiation patterns for the two orthogonal polarizations E_θ and E_ϕ (see Fig. 3) are compared to theoretical radiation patterns in Figs. 6(a) and 6(b). The xy-plane is the plane of the array. The array factor of the patterns was calculated from excitation coefficients given by (9), for measured values of $|S_{21}^m|$ of the elements, as given in Table I. A fourth-order polynomial was fit to the element patterns of $\Lambda = 4.38$, shown in Fig. 4, over the angles $\theta = -55°$ to $\theta = +55°$, and multiplied by the calculated array factor to give the theoretical radiation patterns shown in Figs. 6(a) and 6(b). The agreement between measured and calculated radiation patterns is good over the main beam and first sidelobe. The origin of the 1° offset on the main beam between the measured and calculated patterns of the E_θ polarization is unknown. There is a significant difference between measured and calculated second sidelobe levels. The difference is as much as 4 dB in the second sidelobe level of the E_ϕ polarization. Two sources of this difference are most likely the mutual coupling effects, and the finite return loss of the elements, both of which have been neglected in (7) and (9).

Radiation patterns in the line of the array were also measured at 2.1 and 2.3 GHz. Beam broadening and shoulders on the main beam are consequences of the series feed. The broadside axial ratio at 2.1 GHz is 1.1 dB, and remains less than 1.1 dB over the main beam, while the broadside axial ratio at 2.3 GHz is 2.3 dB and remains less than 2.3 dB over the main beam. The bandwidth for which the radiation patterns were considered useful is 9.1%. To realize the bandwidth of the element with tolerable effects on the array radiation pattern, a corporate feed would be necessary.

Four-port parameters were measured at three spacings for elements 1 and 4 to determine the effects of mutual coupling on the input impedance and $|S_{21}|$ of the elements. The two-port parameters for isolated elements 1 and 4 prior to four-port measurements were $S_{11} = -37.0\angle -70.0°$, $S_{12} = -2.5\angle -70.2°$, $S_{21} = -2.5\angle -70.2°$, $S_{22} = -27.2\angle 147.8°$, and $S_{11} = -20.8\angle 25.3°$, $S_{12} = -2.4\angle -74.3°$, $S_{21} = -2.5\angle -74.6°$, $S_{22} = -21.9\angle 23.7°$, for elements 1 and 4, respectively, with Ports 1 and 2 as shown in Fig. 1. The

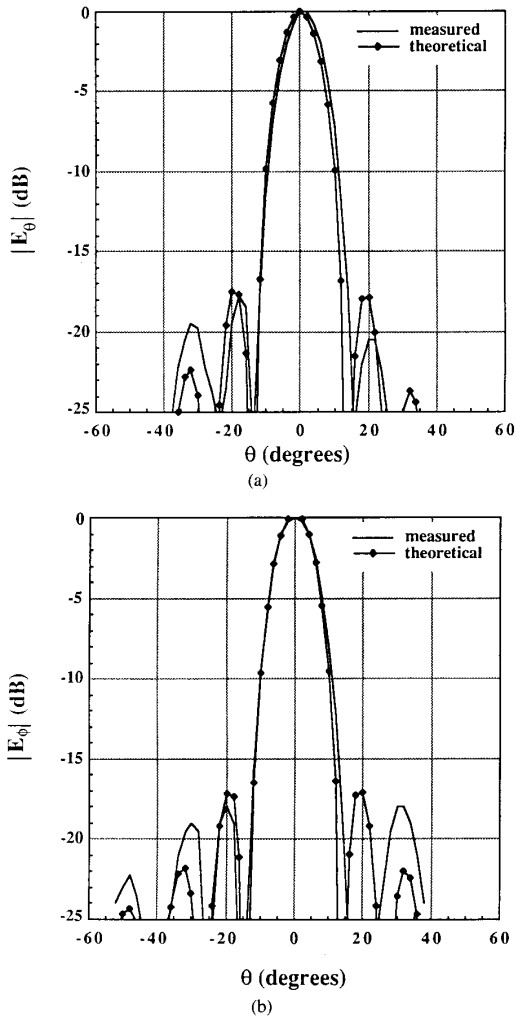

Fig. 6. Comparison of measured and theoretical radiation patterns for the two orthogonal polarizations (a) E_θ, (b) E_ϕ. The ordinate has been normalized such that the main beam maximum is 0 dB.

two-port parameters of the isolated elements can be compared with the analogous parameters in the four-port matrices of Table II. The port numbering for the four-port measurements is shown in Fig. 1 for elements 1 and 4. It is seen that the two-antenna environment has negligible effect on the return loss of the element, and the transmission parameter of the element, for all three spacings given. The parameters $S_{13} = S_{31}$, $S_{24} = S_{42}$, $S_{23} = S_{32}$, and $S_{14} = S_{41}$ are an indication of the mutual coupling between the antennas. The magnitude of these parameters at 0.78 λ spacing is small. These small values, and the relatively small change in the transmission parameter for a single element, while in the two-antenna environment, shows the negligible effect of mutual interactions between the elements at the design spacing. The self-parameters of the elements change little for a decrease from 0.78 to 0.52 λ in element spacing. The $|S_{13}|$, $|S_{23}|$, $|S_{24}|$, and $|S_{14}|$ (and the symmetric parameters) increase with a decrease in spacing. At 0.52 λ element spacing, the largest parameters, $|S_{14}| = |S_{41}|$, and $|S_{23}| = |S_{32}|$ average -18.4 dB.

TABLE II
FOUR-PORT PARAMETERS FOR ELEMENTS 1 AND 4 AT 2.2 GHz

Element Spacing in Wavelengths	$\begin{bmatrix} S_{11} & S_{12} & S_{13} & S_{14} \\ S_{21} & S_{22} & S_{23} & S_{24} \\ S_{31} & S_{32} & S_{33} & S_{34} \\ S_{41} & S_{42} & S_{43} & S_{44} \end{bmatrix}$ (dB) $\angle$ (degrees)			
0.52	$-34.4\angle -49.5$	$-2.4\angle -69.9$	$-22.3\angle -171.2$	$-18.3\angle 164.3$
	$-2.4\angle -69.1$	$-29.4\angle 97.23$	$-18.5\angle 158.3$	$-22.6\angle -172.9$
	$-22.3\angle -171.2$	$-18.5\angle 158.3$	$-20.8\angle 36.2$	$-2.4\angle -74.7$
	$-18.4\angle 163.9$	$-22.6\angle -173.6$	$-2.3\angle -75.5$	$-21.4\angle 41.0$
0.63	$-39.0\angle -20.9$	$-2.2\angle -69.1$	$-29.1\angle 165.5$	$-27.5\angle -123.8$
	$-2.3\angle -69.1$	$-26.8\angle 92.4$	$-27.4\angle 115.7$	$-29.0\angle 167.9$
	$-29.1\angle 164.7$	$-27.4\angle 116.5$	$-19.9\angle 18.5$	$-2.4\angle -75.5$
	$-27.4\angle -127.0$	$-29.0\angle 167.1$	$-2.3\angle -74.7$	$-21.2\angle 19.3$
09.78	$-40.0\angle -57.1$	$-2.3\angle -69.9$	$-34.5\angle 122.1$	$-34.0\angle 71.5$
	$-2.3\angle -69.1$	$-27.1\angle 110.9$	$-34.0\angle 62.7$	$-34.7\angle 125.4$
	$-34.7\angle 122.9$	$-34.0\angle 62.7$	$-21.3\angle 21.7$	$-2.4\angle -75.5$
	$-34.1\angle 72.3$	$-34.7\angle 126.2$	$-2.3\angle -74.7$	$-22.1\angle 21.7$

VI. CONCLUSION

In this paper a simple, inexpensive, CP, series-fed, linear array has been presented. The ability to specify and realize the percentage of the input power that is radiated by an element makes the ANSERLIN antenna an ideal element for a series-fed, low-profile, CP array. Curves relating the percentage of the input power that is radiated by an element to the element geometry were given in the form of $|S_{21}|$ versus Λ.

A technique for the synthesis of radiation patterns using series-fed ANSERLIN elements was given. This technique relates the magnitude of the excitation coefficient to the square root of the power that is radiated by the element. Only design equations that assumed no mutual coupling, and perfectly matched elements, were given. The assumption of identical $|S_{21}|$ for all elements resulted in only fair agreement between the measured and specified radiation pattern. However, a further analysis that did not assume identical $|S_{21}|$ for the elements resulted in good agreement between the measured and theoretical radiation patterns.

The experimental array exhibited a high return loss. A 1.6 dB broadside AR at the design frequency was measured. Improvements in element matching should help reduce the AR by minimizing the reflected waves traveling toward the array feed, which radiate the opposite sense of CP. Finally, the percentage of the input power that was radiated by the array was calculated from measured isolated element parameters to be 86%. This figure depends on the e_A chosen, which in turn must be suitably chosen to give realizable element Λ. The percentage of the input power that is radiated by the array can be significantly increased for many designs.

ACKNOWLEDGMENT

The authors gratefully acknowledge helpful discussions with James Gentle, and the assistance of James Woodruff and Robert Madland in the construction of the array.

REFERENCES

[1] T. Metzler, "Microstrip series arrays," *IEEE Trans. Antennas Propagat.*, vol. AP-29, pp. 174–178, Jan. 1981.
[2] B. B. Jones, F. Y. M. Chow, and A. W. Seeto, "The synthesis of shaped patterns with series-fed microstrip patch arrays," *IEEE Trans. Antennas Propagat.*, vol. AP-30, pp. 1206–1212, Nov. 1982.
[3] W. Dong and D. L. Sengupta, "A class of broadband patch microstrip traveling wave antennas," *IEEE Trans. Antennas Propagat.*, vol. AP-32, pp. 98–100, Jan. 1984.
[4] M. Danielsen and R. Jørgensen," Frequency scanning microstrip antennas," *IEEE Trans. Antennas Propagat.*, vol. AP-27, pp. 146–150, Mar. 1979.
[5] Y. T. Lo, B. Engst, and R. Q. Lee, "Simple design formulas for circularly polarized microstrip antennas," *Proc. Inst. Elec. Eng.*, vol. 135, pt. H, pp. 213–214, June 1988.
[6] J. Huang, "A technique for an array to generate circular polarization with linearly polarized elements," *IEEE Trans. Antennas Propagat.*, vol. AP-34, pp. 1113–1124, Sept.1986.
[7] J. L. Drewniak and P. E. Mayes,"ANSERLIN: A broad-band, low-profile, circularly polarized antenna," *IEEE Trans. Antennas Propagat.*, vol. 37, pp. 281–288, Mar. 1989.
[8] C. S. Liang and Y. T. Lo, "A multipole-field study for the multiarm log-spiral antennas," *IEEE Trans. Antennas Propagat.*, vol. AP-16, pp. 656–664, Nov. 1968.
[9] J. L. Drewniak and P. E. Mayes, "Broadband, circularly polarized radiating-line antennas with an application to a series fed array," Univ. Illinois, Urbana, IL, Electromagn. Lab. Rep. 87-4, 1987.
[10] S. A. Schelkunoff, *Antennas, Theory and Practice*. New York: Wiley, 1952, pp. 160–161.

James L. Drewniak (S'85–M'91), for a photograph and biography please see page 288 of the March 1989 issue of this TRANSACTIONS.

Paul E. Mayes (S'50–M'51–SM'71–F'75), for a photograph and biography please see page 288 of the March 1989 issue of this TRANSACTIONS.